ORIGINAL PAPER

Microfluidic voltammetry: simulation of the chronoamperometric response of microband electrodes sited within microreactors

S. M. Matthews · G. Q. Du · A. C. Fisher

Abstract A computationally efficient fully implicit approach to the simulation of the chronoamperometric response of microband electrodes sited within microscale rectangular ducts is reported. The current response is reported for stagnant solution and where electrolyte is pumped through the cell under microfluidic control. The generality of the method is illustrated with reference to the simple case of a reversible one-electron-transfer reaction. The influence of flow rate and the effects of axial, lateral and normal diffusion upon the electrolysis current are examined and the results compared to approximate analytical behaviour where appropriate.

Introduction

The development of microelectrodes has effectively revolutionised electrochemical measurements, and these tiny devices have demonstrated significant practical benefits over traditional macroscopic electrodes [1–4]. The ability to work in a range of solvents of low polarity, with substantially enhanced rates of mass transport and reduced ohmic distortions have led to a diverse range of analytical applications. In addition, the use of microelectrodes in stagnant solution has permitted examination of fast chemical kinetic processes via rapid scan voltammetric measurements.

S. M. Matthews · G. Q. Du · A. C. Fisher (✉)
Department of Chemical Engineering, University of Cambridge,
New Museums Site, Pembroke Street,
Cambridge, CB2 3RA, UK
e-mail: acf42@cam.ac.uk

The desire to examine increasingly rapid electrolysis reactions has led some workers to combine microelectrode measurements with hydrodynamic techniques. In this paper, the introduction of forced convection extends the time scale of reaction accessible yet further [5–7]. Generally, kinetic and mechanistic information may be derived by either comparison of experimental data with analytical expressions for a specific reaction mechanism or, more usually, the application of numerical models to predict the observed current from the simulated coupled transport/reaction problem. The vast majority of work undertaken within the area has focussed on macroscopic devices, e.g. the channel cell [8].

More recently, we have proposed that the application of microfluidic devices such as microchannels may offer the opportunity to enhance convective transport rates yet further over the macroscopic cells, whilst retaining laminar flow conditions [9–12]. This approach offers the potential to retain the benefits of quantitative analysis via appropriate numerical models with complex microreactor designs where electrode sensors may be incorporated in one or more sites within the cell.

To extract kinetic information from hydrodynamic studies within these devices, we have reported a range of simulation studies for microfluidic devices typically with steady state mass transport [9, 10, 13]. In this article, we extend our work to permit the time-dependent analysis of the chronoamperometric response of microelectrodes embedded in one wall of a duct (see Fig. 1). In cases where the height to width ratio is low, it is necessary to simulate the full three-dimensional velocity and mass transport equations to predict the variation of the current response as a function of the transport rate. In the studies below, we examine the influence of cell height-to-width aspect ratio, solution velocity and mass transport rate on the observed
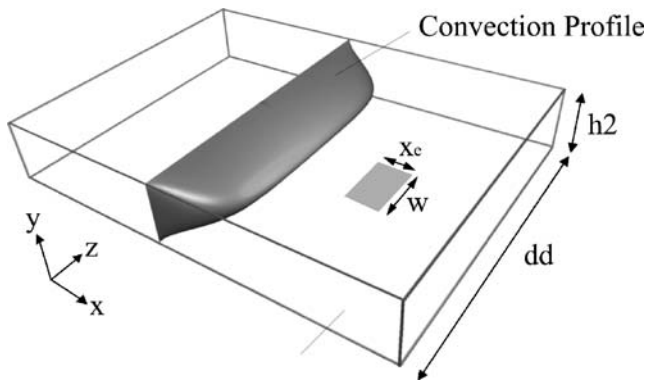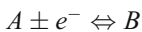
Fig. 1 Schematic diagram of a channel electrode

current obtained during potential step measurements. The extension of the approach to more complex coupled chemical kinetic problems present little conceptual difficulties and offers the potential for these microscopic flow cells to be employed for mechanistic investigations.

Theory

In this section, a theoretical treatment of a potential step simulation is presented for the microreactor system shown in Fig. 1. The current flow for the case of a reversible one-electron electrolysis of a reactant A is considered

$$A \pm e^- \Leftrightarrow B$$

In each simulation, an initial potential is selected where no electrolysis current flows; the potential is then stepped to some final value, which corresponds to the transport-limited reduction/oxidation of species A.

The relevant convective diffusion equation describing the distribution of the reactant A in the cell is given by:

$$\frac{\partial [A]}{\partial t} = D_A \frac{\partial^2 [A]}{\partial x^2} + D_A \frac{\partial^2 [A]}{\partial y^2} + D_A \frac{\partial^2 [A]}{\partial z^2} - v_x \frac{\partial [A]}{\partial x} \quad (1)$$

where D_A is the diffusion coefficient of species A, v_x is the solution velocity in the x-direction as a function of the cell width and the coordinates x, y and z are as defined in Fig. 1. Under conditions of laminar flow, the three-dimensional solution velocity, v_x, can be predicted analytically [14] provided a sufficient lead in length is present to enable the flow to become fully developed [13]

$$v_x = \frac{16\beta^2}{\pi^4} \sum_{n\,(odd)}^{\infty} \sum_{m\,(odd)}^{\infty} \frac{\sin\left(n\pi \frac{\xi}{a}\right) \sin\left(m\pi \frac{\eta}{b}\right)}{nm(\beta^2 n^2 + m^2)}, \quad (2)$$

where a is the width (dd), b is the channel height (h2), β is the height-to-width ratio, ξ is the position along the z axis and η is the position along the y axis. The summation is

performed using $n=1, 3, 5....$ and $m=1, 3, 5 ....$ In all the simulations, it is assumed that sufficient supporting electrolyte is present so that transport effects from migration may be neglected.

The relevant boundary conditions to the problems defined above are

at $t > 0$, $E \ll E_{1/2}$

$x_0 < x < x_0 + x_e, \ y = 0 \quad z_0 < z < z_0 + w$: $[A] = 0$

$x_0 < x < x_0 + x_e, \ y = 0, \quad z_0 < z < z_0$
$+ w : {}^t i = F x_e w D_A (\partial [A] / \partial y)_{y=0}$

$0 < x < x_0, \quad y = 0, \quad 0 < z < dd$: $\partial [A]/\partial y = 0$

$x_0 < x < x_0 + x_e, \ y = 0, \quad 0 < z < z_0$: $\partial [A]/\partial y = 0$

$x_0 + x_e < x, \quad y = 0, \quad 0 < z < dd$: $\partial [A]/\partial y = 0$

$x_0 + x_e < x, \quad y = 0, \quad 0 < z < dd$: $\partial [A]/\partial y = 0$

$0 < x, \quad y = h2, \ 0 < z < dd$: $\partial [A]/\partial y = 0$

$x > 0, \quad 0 < y < h2, \quad z = 0$: $\partial [A]/\partial z = 0$

$x > 0, \quad 0 < y < h2, \quad z = dd$: $\partial [A]/\partial z = 0$

Where x_o and z_o correspond to the start of the electrode in the x and z directions.

To solve Eq. 1, the ADI algorithm is adopted [15], which has been used extensively in electrochemical simulations, and we have demonstrated the approach to macroscopic flow cell techniques [12, 16]. This approach utilises a finite difference grid as shown in Fig. 2, covering the x, y and z directions using increments of Δx, Δy and Δz, respectively. As the problem is symmetrical about the centre axis of the electrode, only half of the cell is used for calculation purposes.

The computational approach proceeds by solving the time-dependent form of Eq. 1 starting from initial boundary conditions. In this case, the cell is initially filled uniformly with a reactant A,

$$t = 0 \text{ all x, all y and all z} [A] = [A]_{Bulk}$$

The time is then incremented in steps of Δt using the counter t^*,
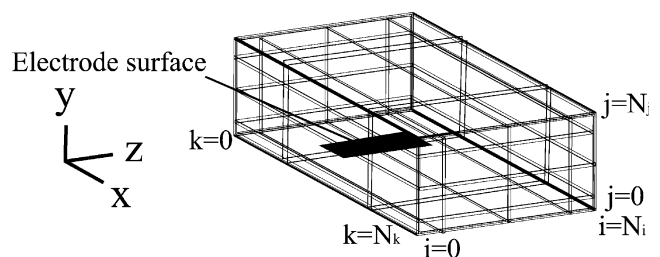
$$t = t^* \Delta t \ t^* = 0, 1, ...T$$

Fig. 2 3D finite difference grid used for channel electrode simulations

The symbol $^t a_{i,j,k}$ is used to denote the normalized concentration of A ($[A]/[A]_{Bulk}$) at the coordinate (i,j,k).

Eq. 2 then becomes

$$\frac{^{t+\Delta t}a_{i,j,k} - {}^t a_{i,j,k}}{\Delta t} = \left(\frac{D_A}{\Delta y^2}\right)\left\{{}^{t+\Delta t}a_{i,j+1,k} - 2^{t+\Delta t}a_{i,j,k} + {}^{t+\Delta t}a_{i,j-1,k}\right\} + \left(\frac{D_A}{\Delta z^2}\right)\left\{{}^{t+\Delta t}a_{i+1,j,k} - 2^{t+\Delta t}a_{i,j,k} + {}^{t+\Delta t}a_{i-1,j,k}\right\}$$
$$+ \left(\frac{D_A}{\Delta x^2}\right)\left\{{}^{t+\Delta t}a_{i,j,k+1} - 2^{t+\Delta t}a_{i,j,k} + {}^{t+\Delta t}a_{i,j,k-1}\right\} - \left(\frac{v_x}{2\Delta x}\right)\left\{{}^{t+\Delta t}a_{i,j,k+1} - {}^{t+\Delta t}a_{i,j,k-1}\right\} \tag{5}$$

Application of the ADI approach enables the above expression to be solved in a fully implicit manner. Rearrangement of (5):

$$\lambda^x = \frac{D_A \Delta t}{\Delta x^2} \tag{6}$$

$$\lambda^y = \frac{D_A \Delta t}{\Delta y^2} \tag{7}$$

$$\lambda^z = \frac{D_A \Delta t}{\Delta z^2} \tag{8}$$

$$\lambda_j^c = \frac{v_x \Delta t}{2\Delta x} \tag{9}$$

and substitution of Eqs. 6, 7, 8 and 9 into 5 yields

$$^{t+\Delta t}a_{i,j,k} - {}^t a_{i,j,k} = \lambda^x\left\{{}^{t+\Delta t}a_{i,j,k+1} - 2^{t+\Delta t}a_{i,j,k} + {}^{t+\Delta}a_{i,j,k-1}\right\}$$
$$+ \lambda^y\left\{{}^{t+\Delta t}a_{i,j,+1,k} - 2^{t+\Delta t}a_{i,j,k} + {}^{t+\Delta t}a_{i,j-1,k}\right\}$$
$$+ \lambda^z\left\{{}^{t+\Delta t}a_{i+1,j,k} - 2^{t+\Delta t}a_{i,j,k} + {}^{t+\Delta t}a_{i-1,j,k}\right\}$$
$$- \lambda_j^c\left\{{}^{t+\Delta t}a_{i,j,k+1} - {}^{t+\Delta t}a_{i,j,k-1}\right\}. \tag{10}$$

Equation 10 was solved at any particular time $(t + t^*\Delta t)$ in three steps. In the first step $(t + \frac{\Delta t}{3})$, the diffusive term in the y-direction was solved implicitly using the Thomas algorithm, whilst the remaining terms are known from either the initial boundary conditions or the previous calculation.

$$^{t+\Delta t}a_{i,j,k} + \lambda^z\left\{{}^t a_{i+1,j,k} - 2^t a_{i,j,k} + {}^t a_{i-1,j,k}\right\}$$
$$+ \lambda^x\left\{{}^t a_{i,j,k+1} - 2^t a_{i,j,k} + {}^t a_{i,j,k-1}\right\} - \lambda_j^c\left\{{}^t a_{i,j,k+1} - {}^t a_{i,j,k-1}\right\}$$
$$= -\lambda^y\left\{{}^{t+\frac{\Delta t}{3}}a_{i,j+1,k}\right\}$$
$$+ (2\lambda^y + 1)\left\{{}^{t+\frac{\Delta t}{3}}a_{i,j,k}\right\} - \lambda^y\left\{{}^{t+\frac{\Delta t}{3}}a_{i,j-1,k}\right\} \tag{11}$$

in the second time interval $(t + \frac{2\Delta t}{3})$, the z-direction components were solved implicitly using

$$^{t+\frac{\Delta t}{3}}a_{i,j,k} + \lambda^y\left\{{}^{t+\frac{\Delta t}{3}}a_{i,j+1,k} - 2^{t+\frac{\Delta t}{3}}a_{i,j,k} + {}^{t+\frac{\Delta}{t}3}a_{i,j-1,k}\right\}$$
$$+ \lambda^x\left\{{}^{t+\frac{\Delta t}{3}}a_{i,j,k+1} - 2^{t+\frac{\Delta t}{3}}a_{i,j,k} + {}^{t+\frac{\Delta t}{3}}a_{i,j,k-1}\right\}$$
$$- \lambda_j^c\left({}^{t+\frac{\Delta t}{3}}a_{i,j,k+1} - {}^{t+\frac{\Delta t}{3}}a_{i,j,k-1}\right) = -\lambda^z\left\{{}^{t+\frac{2}{\Delta t}3}a_{i+1,j,k}\right\}$$
$$+ (2\lambda^z + 1)\left\{{}^{t+\frac{2\Delta t}{3}}a_{i,j,k}\right\} - \lambda^z\left\{{}^{t+\frac{2\Delta t}{3}}a_{i-1,j,k}\right\} \tag{12}$$

and the final time step, the x-direction mass transport components were again solved using

$$^{t+\frac{2\Delta t}{3}}a_{i,j,k} + \lambda^y\left\{{}^{t+\frac{2\Delta t}{3}}a_{i,j+1,k} - 2^{t+\frac{2\Delta t}{3}}a_{i,j,k} + {}^{t+\frac{2\Delta t}{3}}a_{i,j-1,k}\right\}$$
$$+ \lambda^z\left\{{}^{t+\frac{2\Delta t}{3}}a_{i+1,j,k} - 2^{t+\frac{2\Delta t}{3}}a_{i,j,k} + {}^{t+\frac{2\Delta t}{3}}a_{i-1,j,k}\right\}$$
$$= -(\lambda_j^c + \lambda^x)\left\{{}^{t+\Delta t}a_{i,j,k+1}\right\} + (2\lambda^x + 1)\left\{{}^{t+\Delta t}a_{i,j,k}\right\}$$
$$- (\lambda^x - \lambda_j^c)\left\{{}^{t+\Delta t}a_{i,j,k-1}\right\}, \tag{13}$$

so in every full time step $(t+\Delta t)$, the expression is solved implicitly. The simulation proceeds with the application of the relevant boundary conditions described above until a steady state current is established at the working electrode.

The values of $^t a_{i,1,k}$ calculated were used to evaluate the current flowing ($^t i$) at a time t, for any particular flow rate using the following expression

$$^t i = 2FD_A[A]_{bulk}\frac{\Delta x \Delta z}{\Delta y}\sum_{k=k_0}^{k=K}\sum_{i=i_o}^{i=i_w} {}^t a_{i,1,k}, \tag{14}$$

where k_o and i_o are the counters at the start of the electrode in the x and z directions, respectively, with K and i_w being the corresponding boxes at the end of the electrode in the x and z directions. All programmes were written in f77 gcc version 3.3.3 and run on Linux Fedora Core 2.6. Typical run times for the simulations were 24 to 36 h.
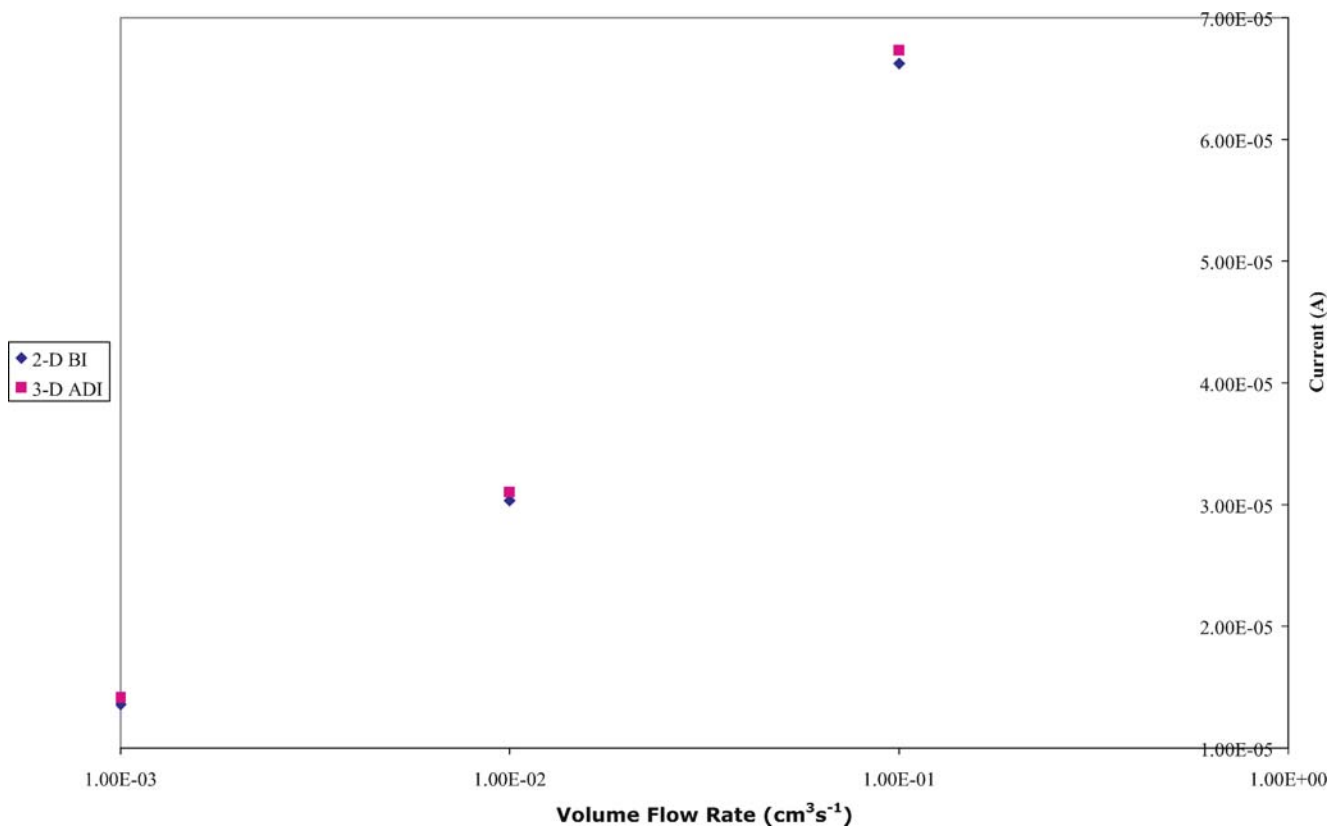
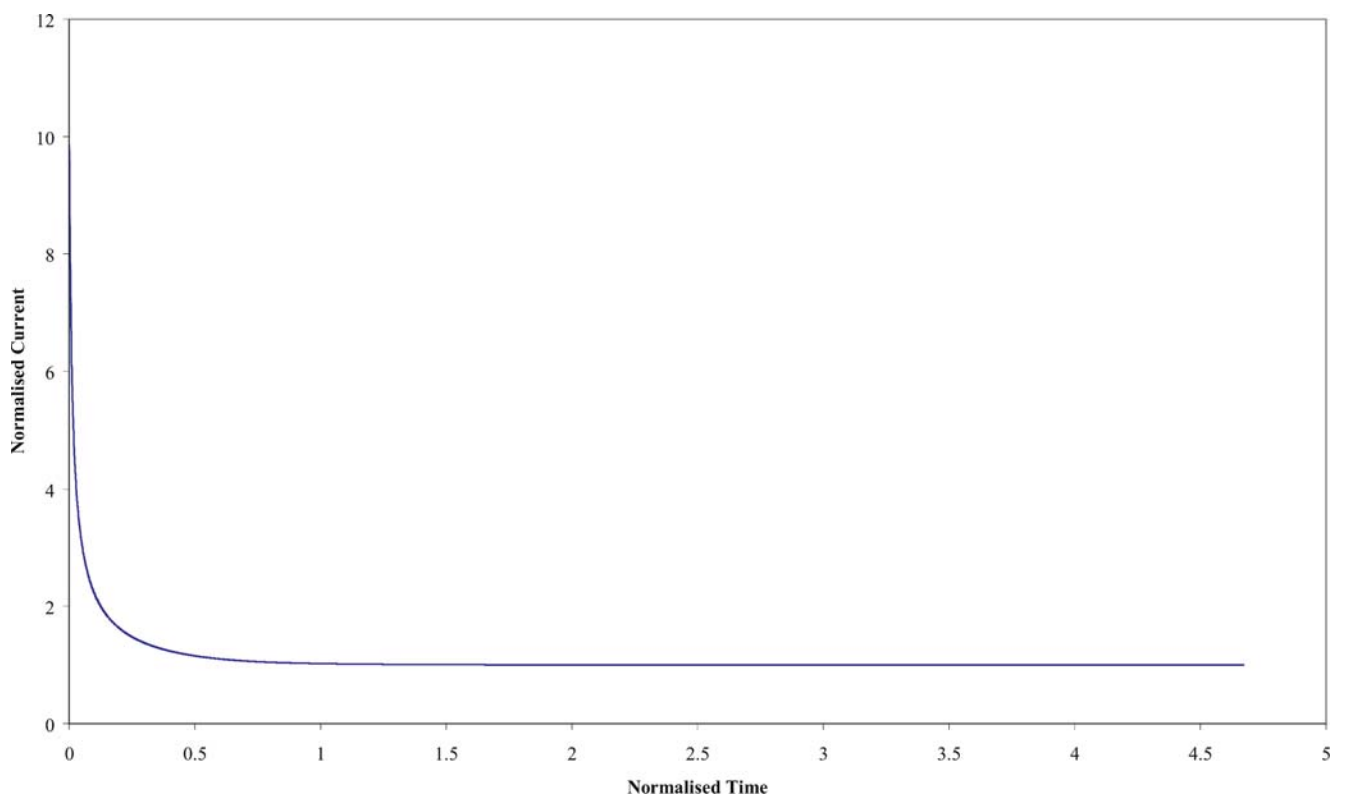**Fig. 3** Variation of transport limited current as a function of volume flow rate

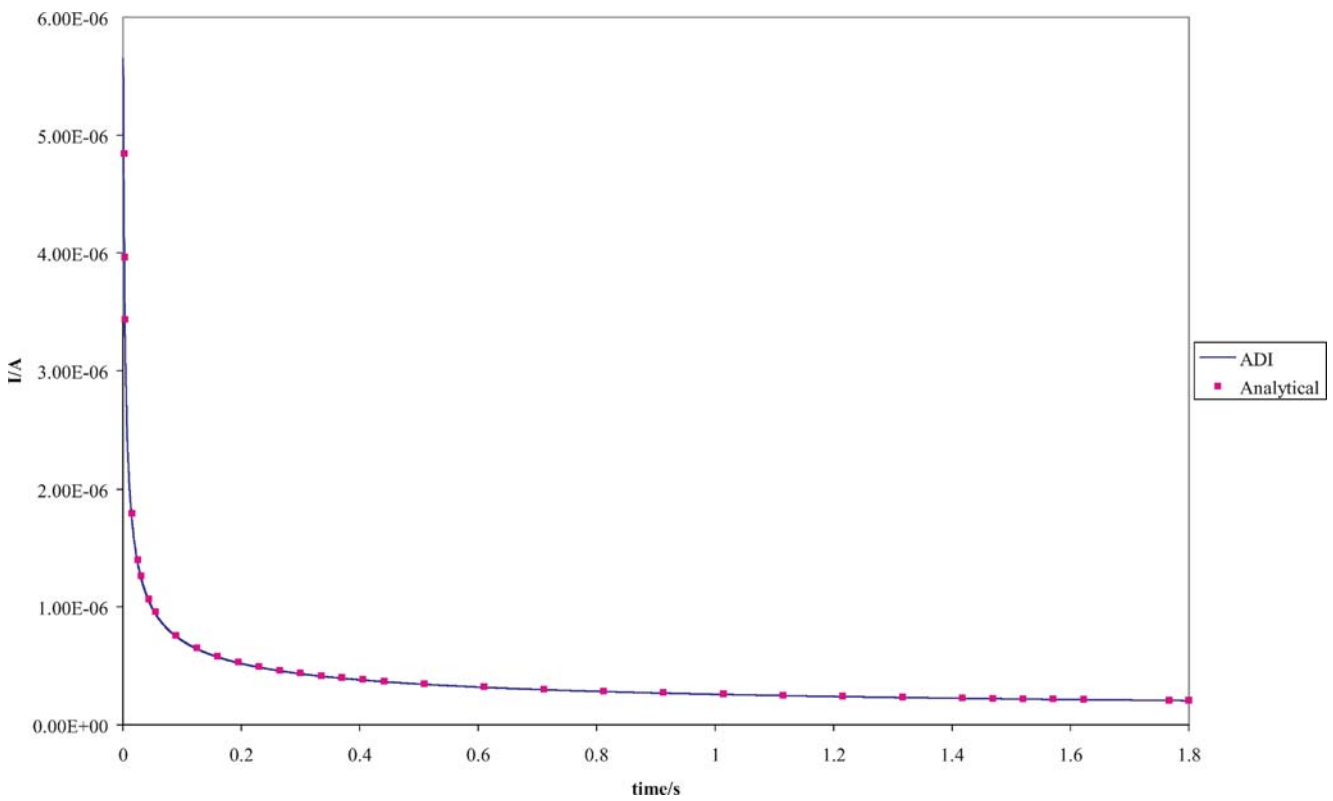**Fig. 4** Normalised chronoamperometric response of channel electrode

Fig. 5 Comparison of chronoamperometric response in no flow conditions to analytically predicted response

Fig. 6 Concentration distributions for 1:1 aspect ratio **a** at the centre of the electrode, **b** 50 μm from the channel wall, **c** 25 μm from the channel wall, and **d** adjacent to the channel wall
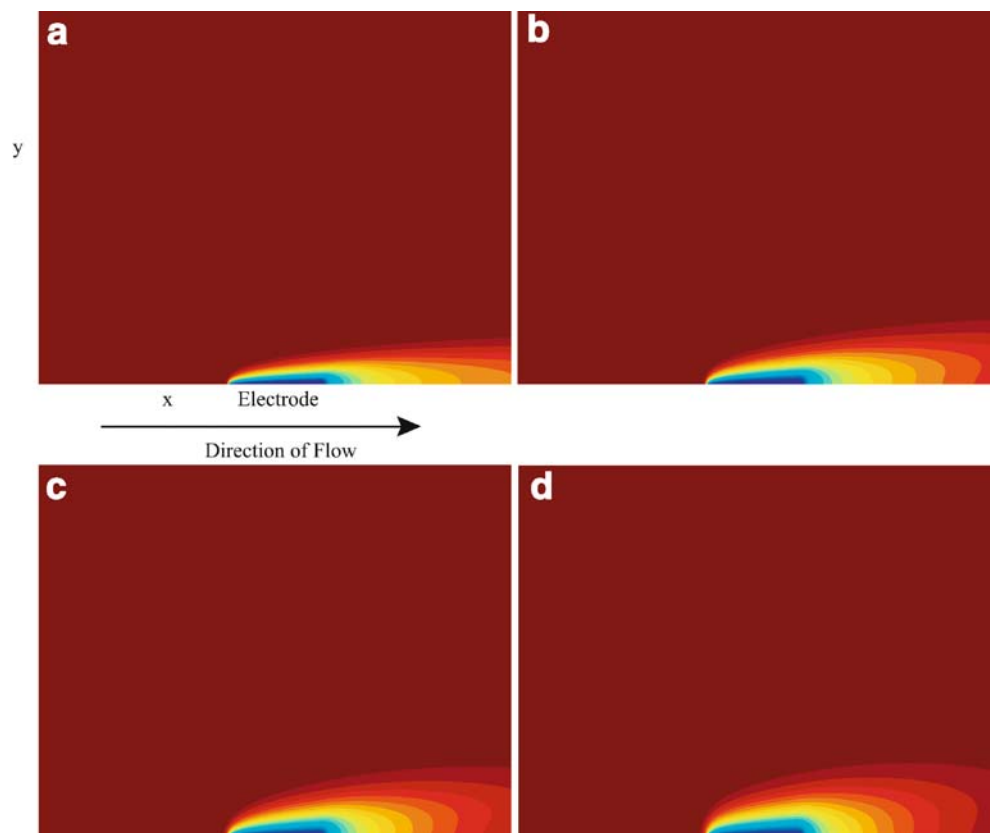
Fig. 7 Concentration distributions for 1:2 aspect ratio **a** at the centre of the electrode, **b** 50 μm from the channel wall, **c** 25 μm from the channel wall, **d** adjacent to the channel wall

Fig. 8 Concentration distributions for 1:10 aspect ratio **a** at the centre of the electrode, **b** 50 μm from the channel wall, **c** 25 μm from the channel wall, **d** adjacent to the channel wall
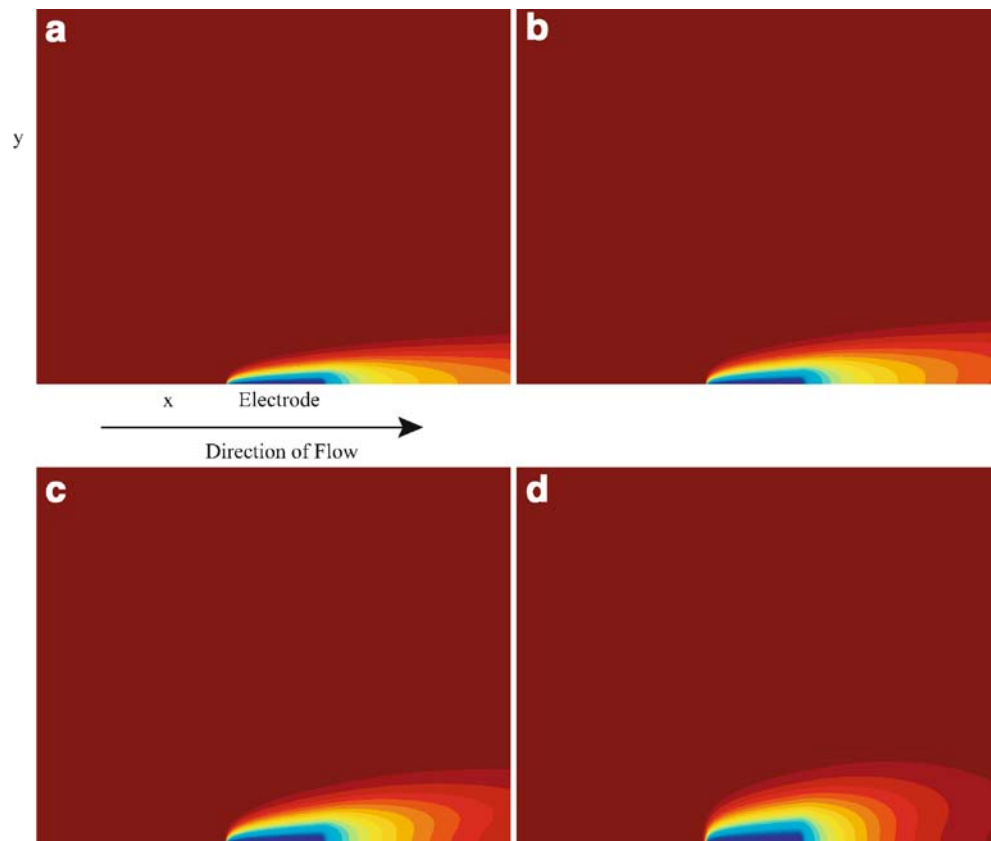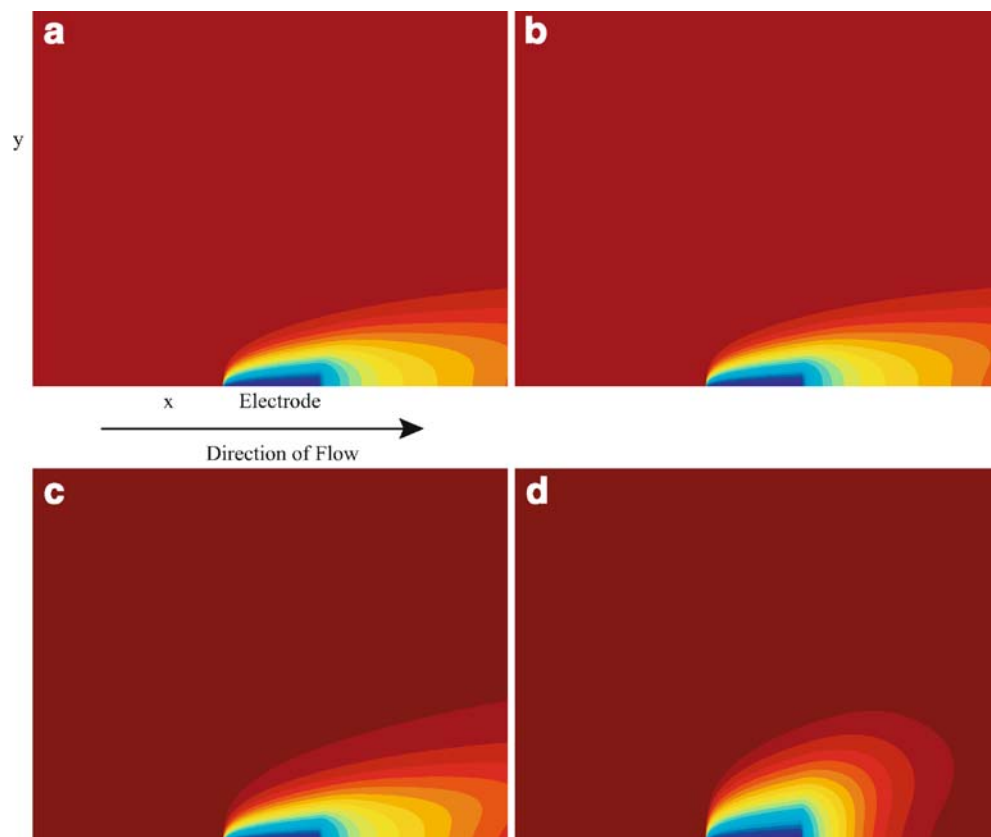
Theoretical results and discussion

To test the numerical codes developed, two cases were assessed for a cell of macroscopic geometry. In this case, a 4×4 mm electrode was sited centrally within the bottom face of a duct of width 0.6 cm, height 0.04 cm. Under these conditions, the hydrodynamic boundary layers at the edge of the cell are sufficiently small that they should render the calculation analogous to a two-dimensional channel flow cell calculation. Figure 3 shows the predicted response for a solution of bulk concentration (of A) of 10^{-6} mol cm^{-3} and with a diffusion coefficient of 10^{-5} cm^2 s^{-1}, using the following parameters: $\Delta t = 0.05$, $N_I = 20$, $N_K = 100$, $N_J = 200$ (increasing the grid parameters employed was found to produce no significant difference (<1%) in the calculated currents), with volume flow rates 10^{-1}, 10^{-2} and 10^{-3} cm^3 s^{-1}.

Under these conditions, it is established that axial convection and diffusion normal to the electrode surface are the dominant transport characteristics and, therefore, control the mass transport limited current. It is possible to routinely predict the current flowing under these conditions using a backwards implicit (BI) approach described previously [15]. Also presented in Fig. 3 is the current predicted on the basis of the BI calculations. Excellent agreement is observed between the two approaches, highlighting the accuracy of the two-dimensional approximation inherent in the BI calculations for these wide-aspect-ratio cells and the flow rate range chosen.

The BI strategy also permits the chronoamperometric response [15] to be predicted as a function of volume flow rate at a macroelectrode. The ADI approach was again used and the potential was stepped from an initial potential where no current flows to a value corresponding to mass transport limited behaviour. Figure 4 shows the computed values using the ADI approach for the same geometry as above with $\Delta t = 0.005$, $N_I = 20$, $N_K = 40$, $N_J = 200$ and for volume flow rates of 10^{-1}, 10^{-2} and 10^{-3} cm^3 s^{-1}. In each case, good agreement is found between the values calculated and those predicted using the BI approach.
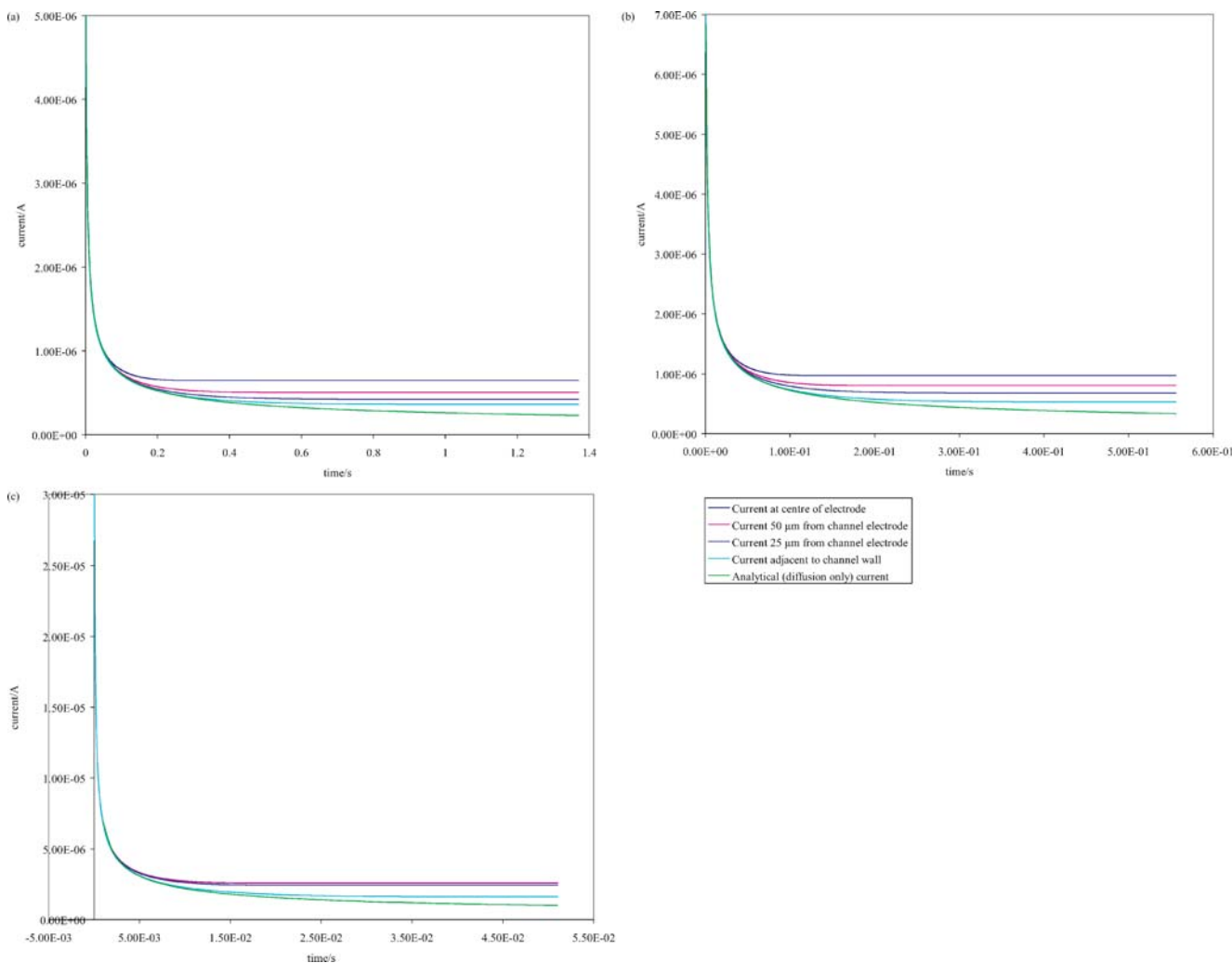

Fig. 9 Chronoamperometric response for different positions across the electrode for **a** 1:1 aspect ratio, **b** 1:2 aspect ratio, **c** 1:10 aspect ratio

The normalised current is calculated as $\frac{I}{I_{lim}}$ and normal-ised time is $\left(\frac{4V_0 D_A}{x_e^2 \left(\frac{h_2}{2}\right)^2}\right)^{\frac{1}{3}}$ where V_0 is $\left(\frac{3V_f}{4\left(\frac{h_2}{2}\right)dd}\right)^2 V_f$ in this instance is taken as the flow rate in the central pixel of the flow profile.

As a final check, numerical simulations were performed using the ADI algorithm under conditions of no flow with a microelectrode of length 250 μm and width 500 μm. Under these conditions, the chronoamperometric response of a microband electrode is known approximately analytically [16]. Figure 5 shows the transients computed using the ADI algorithm (Δt=0.00008, N_I=150, N_K=100, N_J=250) and from the analytical expression given in [16]. A diffusion coefficient of 10^{-5} cm^2 s^{-1} was assumed. Again excellent agreement is obtained using the strategy described, illus-trating the satisfactory nature of the approach.

Next simulations were performed to assess the effect of the hydrodynamic boundary layer established when the cell width-to-height ratio is no longer large and edge effects might be expected to alter the chronoamperometric behav-iour from the simple-dimensional models. In the cases below, we simulate three different aspect ratio cells, (1:1,

1:2, 1:10) for flow rates and experimental conditions, which are typically employed for these types of devices.

First potential step simulations were carried out for the three aspect ratios noted above, the width of the channel was fixed at 500 μm and the height was varied from 500 μm (1:1) to 50 μm (1:10) using an electrode 250 μm long, which spanned the full width of the channel, and with the grid parameters Δt=0.00008, N_I=150, N_K=200 and N_J=250. Figures 6, 7 and 8 show the steady-state concentration distributions for the different cell-aspect ratios as a function of position across the width of the electrode. All of the data displayed below was obtained with a volume flow rate of 10^{-3} cm^3 s^{-1}.

The plots reveal a significant broadening of the diffusion profile within the hydrodynamic boundary layer region as anticipated, which was most significant for the 1:1 aspect ratio. A quantitative examination of the current density was performed for various strips across the electrode width. Figure 9 reveals the chronoamperometric response for different electrode strips taken at $0<x<x_e$, z=centre of electrode, 50 μm from the channel wall, 25 μm from the channel wall and adjacent to the channel wall. In each plot, the chronoamperometric response is compared to that
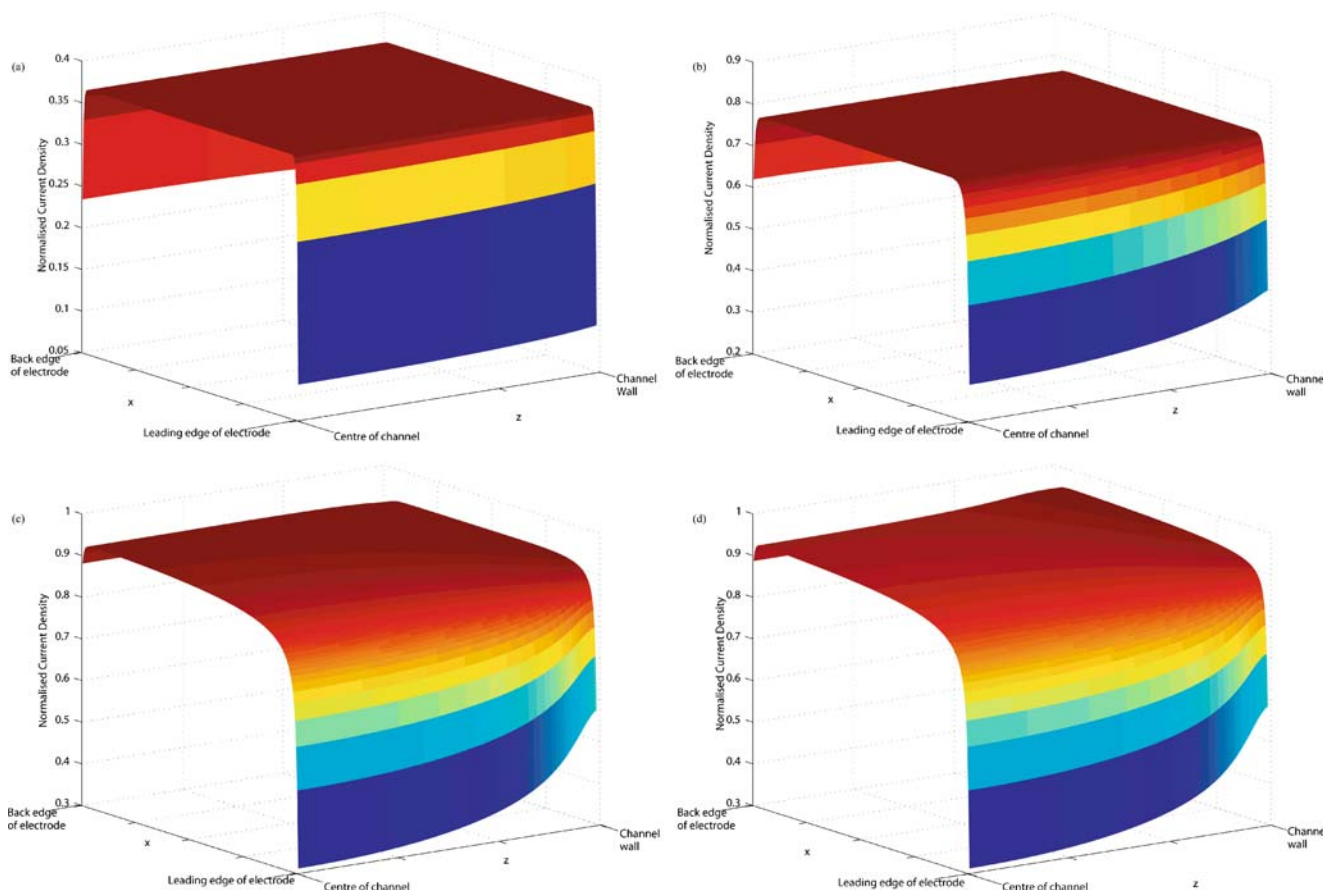

Fig. 10 Current density maps for aspect ratio 1:1 at **a** t=0.0008 s, **b** t=0.008 s, **c** t=0.08 s, and **d** t=1.3 s (steady state)

predicted analytically [16]. It is apparent that the central region of all the cells gives a good agreement with the prediction for a cell of infinite width. When in the hydrodynamic boundary layer, the chronoamperometric behaviour begins to tend towards that of a pure diffusion problem for a microband.

Finally, a current map as a function of time was examined for each aspect ratio. Figure 10 reveals the observed response for the 1:1 aspect ratio cell. The transient reveals an almost totally uniformly accessible electrode at short times, which evolves into the limiting behaviour at steady state shown in Fig. 9.

The substantial edge effects observed due to the hydrodynamic boundary layer for this aspect ratio highlight the need for a full three-dimensional treatment of the convective diffusion problem.

Conclusions

Transport limited, chronoamperometric behaviour at hydrodynamic microband electrodes may be efficiently predicted using the ADI algorithm to solve the relevant mass transport equations. In particular, the influence of lateral and axial diffusion is found to be substantial for the flow rates investigated (10^{-1} to 10^{-3} cm^3 s^{-1}) for microband electrodes of 250 μm length. Quantitative agreement was found between experimental and theoretical predictions for steady state and chronoamperometric measurements. The highly non-uniform diffusion layer generated around the microband electrode offers the potential to develop this new device yet further to examine complex mechanistic processes. Further work is currently underway into the application of these new devices to the investigation of rapid electrochemical reactions using a combination of rapid scan and hydrodynamic techniques.

References

1. Fleischman M, Pons S (1987) Ultramicroelectrodes. Datatech, Morganton, NC
2. Wang J (1990) Microelectrodes. VCH, New York
3. Bond AM (1994) Analyst 119:1
4. Cooper JB, Bond AM, Oldham KB (1992) J Electroanal Chem 331:877
5. Compton RG, Fisher AC, Wellington RG, Dobson PJ, Leigh PA (1993) J Phys Chem 97:10410
6. Compton RG, Dryfe RAW, Alden JA, Rees NV, Dobson PJ, Leigh PA (1994) J Phys Chem 98:1270
7. MacPherson JV, Macar S, Unwin PR (1994) Anal Chem 66:2175
8. Booth J, Compton RG, Cooper JA, Dryfe RAW, Fisher AC, Davies C, Walters M (1995) J Phys Chem 99:10942
9. Sullivan SP, Johns ML, Matthews SM, Fisher AC (2005) Electrochem Commun 7:1323
10. Henley IE, Fisher AC (2003) J Phys Chem B 107:6579
11. Yunus K, Henley IE, Fisher AC (2003) J Phys Chem B 107:3878
12. Yunus K, Fisher AC (2003) Electroanalysis 21:15
13. Henley IE, Fisher AC (2003) Electroanalysis 21:55
14. Spiga M, Morini GL (1994) Int Commun Heat Mass Transf 21:469
15. Fisher AC, Compton RG (1991) J Phys Chem 95:7539
16. Aoki K (1993) Electroanalysis 5:627